Journal of Computational Electronics (2022) 21:361–377
https://doi.org/10.1007/s10825-022-01851-7

Design of a D-π-A-A framework with various auxiliary acceptors on optoelectronic and charge transfer properties for efficient dyes in DSSCs: A DFT/TD-DFT study

Lala Adetia Marlina[1,2] · **Winarto Haryadi**[2] · **Harno Dwi Pranowo**[1,2]

Received: 22 April 2021 / Accepted: 2 January 2022 / Published online: 15 February 2022

Abstract

Derived from an excellent light harvester, an iminodibenzyl-substituted porphyrin sensitizer consisting of a series of D-π-A-A structural motifs, was investigated using density functional theory (DFT) and time-dependent DFT methods to demonstrate the effects of various auxiliary acceptors on sensitizers. Absorption spectra simulations at 417.51 nm calculated using CAM-B3LYP with a mixed LanL2DZ/6-31G(*d*,*p*) basis set exhibited good agreement with the experimental results (i.e., 426.60 nm). Impressively, the introduction of a co-acceptor moiety on the sensitizers effectively shifted the light absorption to the NIR region. The computational results showed that Dye 9 notably exhibited the smallest HOMO–LUMO energy gap (3.34 eV). The *Q* band of Dye 9 was located at 756.72 nm, which was the largest wavelength and the most redshifted absorption spectrum. The short-circuit current density (J_{SC}) was calculated by considering the free energy of charge injection (ΔG_{inject}), the free energy of dye regeneration (ΔG_{reg}), and light-harvesting efficiency (LHE). The oscillator strength of the maximum absorption was greatest for Dyes 3 and Dye 9, resulting in increase LHE and improved J_{SC}, hence affecting the overall photoelectric conversion efficiency. Dye 9 demonstrated better electron transfer performance, with q_{CT} (0.630 e^{-}), which was attributed to its better planarity compared to other dyes. Interestingly, Dye 9 exhibited substantially enhanced nonlinear optical response through intramolecular charge transfer process, with a β_{tot} value many-fold higher than that of urea computed at the same theoretical level. It indicates that the studied dye molecules are potential candidates for the optoelectronic applications. Dye 9 was therefore the most feasible dye candidate for efficient DSSC applications.

Graphical abstract

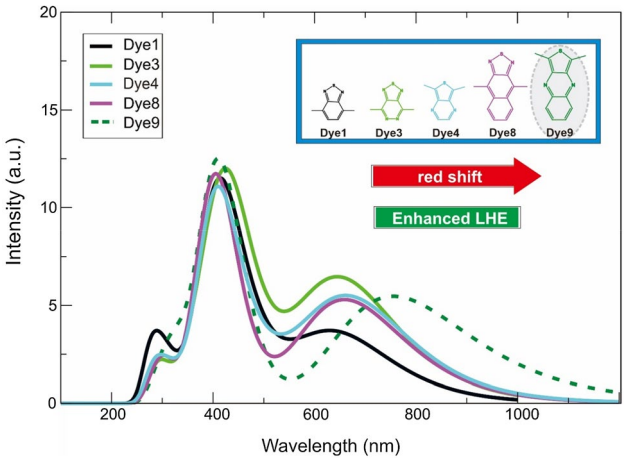

Keywords Iminodibenzyl · Porphyrin · DFT and TD-DFT · Electronic and optical properties · DSSCs

Extended author information available on the last page of the article

1 Introduction

Dye-sensitized solar cells (DSSCs) are considered a viable alternative for harvesting of infinite solar energy resources for future energy needs, and many studies have been carried out on both theoretical aspects and fabrication of the device [1]. Historically, extensive research has been conducted on DSSCs since they were introduced by O'Regan and Gratzel in 1991 [2], due to their acceptable efficiency and photophysical and electrochemical properties that can be effectively managed. DSSCs are also regarded as a promising encouraging alternative for photon capture and charge transport in solar conversion [3].

DSSCs typically contain four elements: a mesoporous working electrode (as part of the photon anode), a dye (connected to the surface of the oxide semiconductor), a redox liquid electrolyte (based mostly on iodine electrolytes), and a counter electrode. Dyes play a pivotal role in DSSCs, as they are responsible for the wide range of light absorption from the ultraviolet–visible (UV–Vis) to the infrared (IR) region and for capture of abundant solar energy to generate electricity and mediate the interactions between semiconductors and redox transport [4–6].

To date, Ru(II) and Zn(II) porphyrin complexes have demonstrated outstanding photophysical properties due to their wide suitability, and display impressive power conversion efficiency (PCE) of 11% and 13%, respectively [7, 8]. The utilization of ruthenium complexes in DSSC applications is still limited, mainly because of their high cost due to their limited resources [9, 10]. Meanwhile, due to the high molar absorption coefficient in both blue (Soret band at 350–500 nm) and red (Q band at 550–700 nm), porphyrin can be an excellent light harvester [11–13].

Among dye sensitizers, the efficient push–pull D-π-A system, which represents the D (donor), π (bridge), and A (acceptor) configuration, is responsible for the PCE of DSSCs. A better intramolecular charge transfer (ICT) phenomenon and separation on photoexcitation are affected by the electron-donating capability of the donor unit, the ability of the acceptor to withdraw electrons, and the modification of the length or shape of the π spacers [14].

Therefore, improved photovoltaic performance can be achieved by adjusting the molecular structure and optimizing energy levels. A modification of the D-π-A framework leads to a dye structure which is more effective than the basic D-π-A structure. For instance, SM315 and SM371 significantly improve UV–Vis and near-infrared (NIR) absorption through insertion of multiple triple bonds between the porphyrin core and the anchoring group; efficiency of up to 13% was recorded in 2014 [7]. In the same context, Wang et al. also effectively integrated a porphyrin sensitizer and an ethynyl unit to achieve high PCE of up to 10.45% in the presence of an iodide/triiodide-based electrolyte [12]. This record was exceeded by a PCE value of 12.5% for a C275 dye with the insertion of an ethynyl unit to form an interpenetrating charge transport network [15]. Ethynyl units have since been widely used to connect porphyrin cores for constructing several new kinds of sensitizers, which can facilitate the electronic coupling on the TiO_2 surface and widen the light-harvesting regions [10]. A study by Song et al. showed that insertion of an ethynyl unit proved highly effective for increasing light absorption and enhancing photovoltaic performance in comparison to counterpart dyes without insertion [16].

In a separate study, the introduction of the co-acceptor moiety into the D-π-A system to form a D-π-A-A structural motif not only affected the electron withdrawal ability, but also improved the light-harvesting ability. Reports in the literature reveal that the insertion of a double acceptor moiety in the dye structure can also widen the absorption band. Slimi et al. investigated a new type of D-π-A-A organic dye with a triphenylamine derivative as the core and benzoic acid as the anchoring group within the BH and HLYP/6-31G(*d*, *p*)/SMD level, in which dye D4 contained 1,2,5-thiadiazolo[3,4-*d*]pyridazine units as an auxiliary acceptor, exhibiting better photovoltaic properties [17]. Recently, Zhao et al. studied five D-π-A-A organic dyes of heterocyclic polycyclic aromatic hydrocarbons (hetero-PAH). The results showed that the introduction of indoline derivatives (B) as a donor group or benzobisthiadiazole (B) as an auxiliary acceptor unit can improve the photoelectric performance [18]. Previous studies have shown that a series of auxiliary acceptors including benzotriazole [19, 20], quinoxaline [21–23], and benzothiadiazole [1, 24–26], among others [27–30], can be employed to expand the light-harvesting response of the dye.

High-level quantum chemical techniques are useful in the design of efficient sensitizers, as they determine the properties of electron transfer, charge separation, injection, and regeneration processes. From a theoretical perspective, a number of studies have explored density functional theory (DFT) and time-dependent DFT (TD-DFT) for the rational design of molecular modification of the donor, π-spacer, and acceptor units [31–34]. Using the DFT/B3LYP/LANL2DZ method, computational studies have been carried out on the effect of substituent groups on the molecular and electronic structures of several meso-substituted metalloporphyrin complexes. The results of the calculations show that the introduction of the substituent groups in metalloporphyrin (Cd-, Hg-, and Pt-porphyrin) has a significant effect on the electronic properties [35–37].

D-π-A dye molecules with an iminodibenzyl (IDB)-substituted porphyrin sensitizer were synthesized and exhibited photo-conversion efficiency (PCE) up to 5.26%, short-circuit current density (J_{SC}) of 9.68 mA cm^{-2}, open-circuit

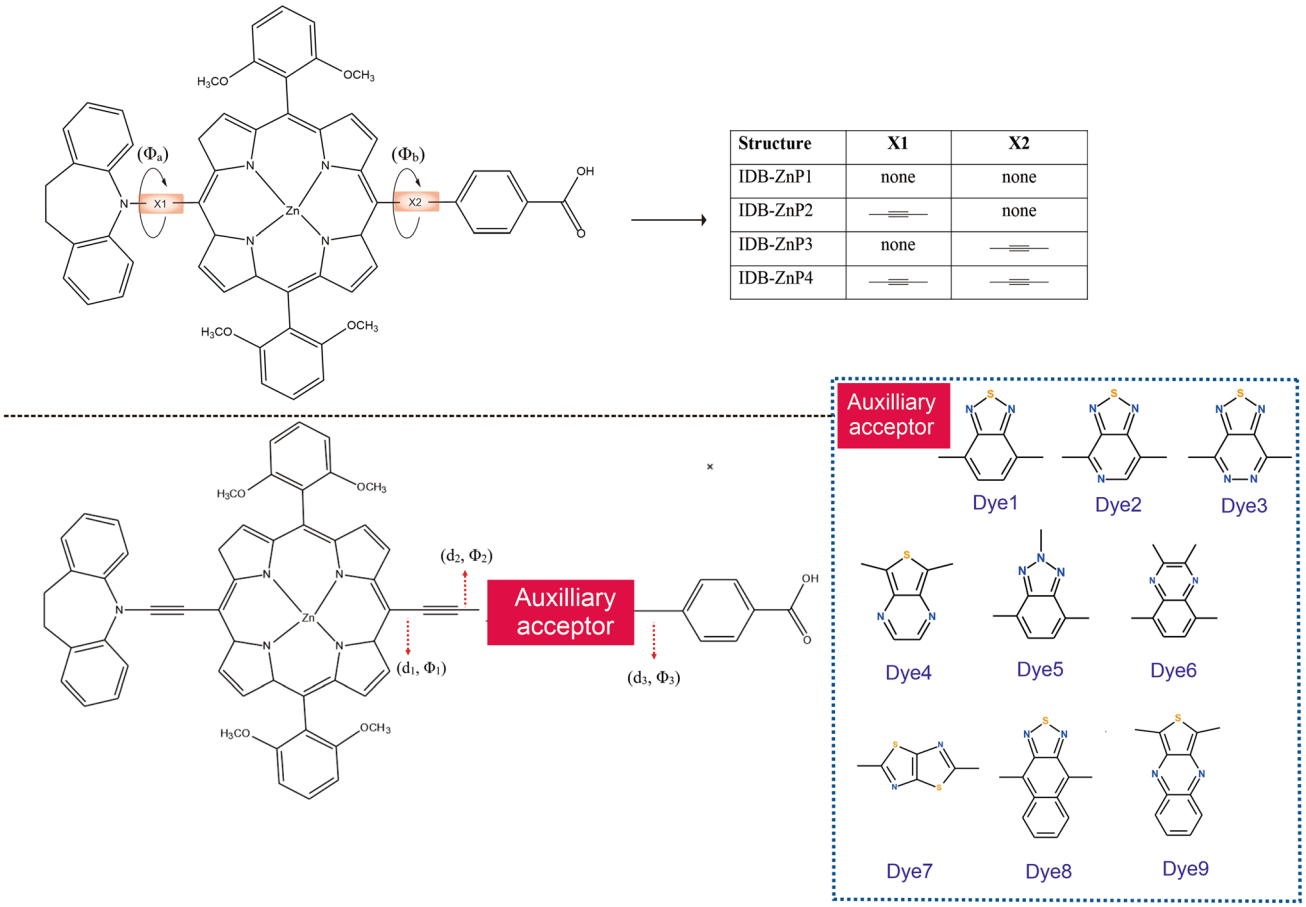

Fig. 1 Molecular structure of the studied dyes

photovoltage (V_{OC}) of 0.74 V, and fill factor (FF) of 0.73, thus demonstrating better performance than diphenylamine (DPA)-substituted porphyrin and iminostilbene (ISB)-substituted porphyrin, with PCE of 4.05% and 2.62%, respectively [38]. Based on this study, it appears that IDB is a potential electron donor for photovoltaic applications.

In this paper, to study the effect of the molecular structure on photovoltaic performance, we compared the performance of a series of dyes with IDB-substituted porphyrin sensitizer reference dyes (IDB: 5.26%). As exhibited in Fig. 1, a D-π-A-A series of IDB-substituted porphyrin sensitizers with different auxiliary acceptors was designed to examine the relationship between the expanded acceptor moieties and the performance of DSSCs. The porphyrin core in the meso position was linked by ethynyl units to this latter group. We introduced benzo[c][1,2,5]thiadiazole, [1,2,5]thiadiazolo[3,4-*c*]pyridine, [1,2,5]thiadiazolo[3,4-*d*] pyridazine, thieno[3,4-*d*]pyridazine, 2-methyl-2H-[1,2,3] triazolo, 2,3-dimethylquinoxalin, thiazolo[5,4-*d*]thiazole, naphtho[2,3-*c*][1,2,5]thiadiazole, and thieno[3,4-*b*]quinoxaline as auxiliary acceptors between the ethynyl unit and the anchoring group (see Fig. 1). Because of their high conjugation of π electrons and planarity, these units were selected and expected to trap electrons in order to increase the mobility of the charge carriers from the electron-donating to the electron-accepting groups.

The dyes designed by forming the D-π-A-A configuration exhibited better electronic and optical properties, as well as a decrease in the bandgap, indicating that the dye designed in this work exhibited better performance. The effect on the electron injection and dye regeneration processes was ascertained by the calculated energy gap trends of these dyes, which are high compared with the spectral data. Furthermore, our theoretical study is expected to serve as a stepping stone into a new design of metalloporphyrin-based dye molecular optimization for future applications in DSSCs**.**

2 Computational details

In summary, all isolated dyes in neutral, cationic, and anionic states were optimized in the frame of DFT with CAM-B3LYP using the LANL2DZ basis set for Zn atoms and 6-31G(*d*,*p*) for other atoms [39]. To obtain the absorption

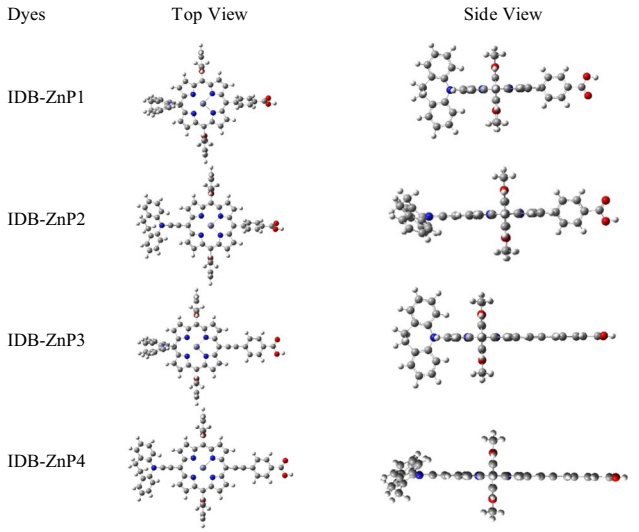

Fig. 2 The optimized geometry structure using DFT/CAM-B3LYP with the 6-31G(*d*,*p*) (LANL2DZ for Zn atoms) basis set THF solvent. The color scheme adopted is gray, white, blue, red, yellow, and light blue for C, H, N, O, S, and Zn atoms, respectively

spectrum simulation in a more realistic environment, the above optimization was achieved in tetrahydrofuran (THF) solvent with the conductor-like polarizable continuum model (CPCM) [40–42]. The electronic excitation and absorption energy of the spectrum of the organic dye molecules was calculated using TD-DFT. The six XC functions investigated were B3LYP [43], CAM-B3LYP [44], M06 [45], ωB97XD [46], BH and HLYP [47], and MPW1PW91 [48], while the basis sets for organic atoms including 6-31G, 6-31G(*d*), 6-31G(*d*,*p*), 6–31++G, 6–31+G(*d*,*p*), and 6–31++G(*d*,*p*) were also investigated. These basis sets are widely used and efficiently reproduce many of the electronic properties, i.e., geometric parameters for organic atoms, including charge transport and nonlinear optical (NLO) properties [49–53].

The resulting simulated absorption spectra produced using various functions and basis sets were compared with the reference absorption spectra for IDB [38] (see Supplementary Information Table S2). Considering the smallest deviation of the absorption spectrum through experiments, the UV–Vis absorption spectra analysis for IDB was obtained using CAM-B3LYP with LanL2DZ/6-31G(*d*,*p*). Thus, it is the most reliable function and basis set to investigate the photophysical properties. Based on these findings, the CAM-B3LYP with LanL2DZ/6-31G(*d*,*p*) was applied in this work.

All calculations were performed using the Gaussian09 program package [54]. To analyze the different phenomena of charge transfer properties during electron transitions, the charge transfer parameters were calculated with CAM-B3LYP/6-31G(*d*,*p*) and LANL2DZ (for Zn atoms) using the method developed by Ciofini et al. [55, 56] implemented in Multiwfn 3.3.8 code [57]. Moreover, the NLO properties were computed with the CAM-B3LYP using the same basis set, mixed LanL2DZ/6-31G(*d*,*p*) in gas phase.

3 Results and discussion

3.1 Geometric structure properties

In this study, we designed several different dyes based on experimentally studied dyes with the D-π-A-A system, which takes iminodibenzyl as the donor electron, porphyrin as π-spacer, and benzoic acid as the anchoring unit. For molecular rigidity, the donor and anchoring units are attached to the π-spacer, respectively, by an ethynyl bridge (carbon–carbon triple bond). In addition, several different auxiliary acceptors were selected and are fitted between the π-spacer–ethynyl bridge unit and the anchoring unit to increase the planarity and the potential for the conjugate effect.

To evaluate the effect of insertion of the ethynyl bridge and different auxiliary acceptor units, the optimized geometries of the dyes, which were obtained using DFT/CAM-B3LYP with the 6-31G(*d*,*p*) (LANL2DZ for Zn atoms) basis set in THF solvent, are presented in Fig. 2, and the selected geometric parameters are tabulated in Table 1. The Cartesian coordinates of the optimized ground-state geometries of the dyes are provided in the supporting material.

As presented in Fig. 1, d_1 and Φ_1 are the bond lengths and dihedral angles between the Zn–porphyrin ring as the π-bridge and the triple bond (ethynyl units), respectively. Φ_2 and d_2 are the dihedral angles and bond lengths between the ethynyl unit and the auxiliary acceptor (*A*), respectively. Φ_3 is the dihedral angle between the auxiliary acceptor and benzoic acid (anchoring group), while d_3 is the corresponding bond length of the auxiliary acceptor and the anchoring group. Based on the results of observational data, the bond distance values between the single and double bonds obtained for d_1, d_2, and d_3 are in the range of 1.400–1.483 Å for all dyes, which indicates that these bond lengths are shorter than the C−C single bond. This suggests that these bond lengths have a double bond (C=C) character (i.e., C–C: 1.506 Å, C=C: 1.446 Å) [58], which contributes to the small energy gap (Δ_{H-L}). Moreover, this means that there is delocalization of π electrons between each of the constituent groups of the molecule.

None of these dyes is particularly planar. It can be seen from Table 1 that IDB-ZnP4 has better coplanarity than IDB-ZnP1. This indicates that the optimized ground state of IDB-ZnP4 consists of donor and acceptor moieties that separate the Zn–porphyrin ring from the ethynyl bridges on the left and right side, which keeps the molecules in

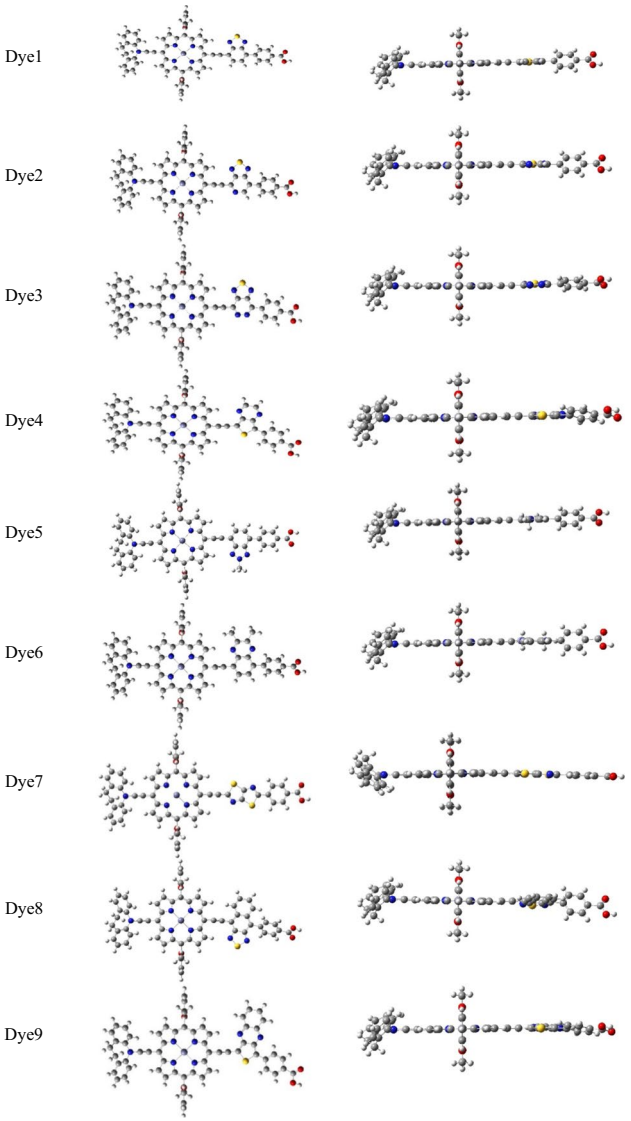

Fig. 2 (continued)

one plane. The larger dihedral angles resulting from the mutual exclusion of iminodibenzyl and Zn–porphyrin/Zn–porphyrin and benzene are bridged by a triple bond (C≡C).

On the other hand, the dihedral angles of Φ_1, Φ_2, and Φ_3 are in the same plane (in the order of ~ 180°), due to the extended π-bond conjugation for Dyes 1–9. Because of the introduction of an ethynyl bridge and suitable auxiliary acceptors, this will improve the planarity between the π-bridge and the anchoring unit. In general, it is known that the more planar the dye molecules are, the greater the injection of the photoexcited electrons from the dye into the conduction band (CB) of the semiconductor surface. Based on the above explanation, Dye 9 displays excellent molecular planarity compared to other molecules (see dihedral angle $\Phi_{1,2,3}$ ~ 163–173° in Table 1). This suggests that Dye 9 might lead to a broad redshift at the maximum absorption wavelength and show better photovoltaic performance.

3.2 Electronic structure properties

The proper highest occupied molecular orbital (HOMO) and lowest unoccupied molecular orbital (LUMO) energy levels of the sensitizer are good tools for predicting electronic transition behavior and excitation properties [59]. To better understand the effect of introducing auxiliary acceptors on the electronic properties of these dyes, quantum chemical calculations were carried out on the investigated dyes. Through systematic tuning of the optical and electronic properties of the dye, it is possible to achieve the desired properties for maximum power conversion efficiency of the DSSCs. The $E_{\text{HOMO-1}}$, E_{HOMO}, E_{LUMO}, $E_{\text{LUMO+1}}$, and the HOMO–LUMO energy gap ($\Delta_{\text{H–L}}$) of the different studied dyes are collected in Table 2 and illustrated in Fig. 3.

Table 1 Selected bond distance (unit in Å) and dihedral angle (unit in °) of the studied dyes

Dye	Bond length			Dihedral angle				
	d_1	d_2	d_3	Φ_a	Φ_b	Φ_1	Φ_2	Φ_3
IDB-ZnP1	–	–	–	99.74	114.02	–	–	–
IDB-ZnP2	–	–	–	179.761	114.31	–	–	–
IDB-ZnP3	–	–	–	100.02	179.86	–	–	–
IDB-ZnP4	–	–	–	177.77	179.67	–	–	–
Dye 1	1.422	1.417	1.479	–	–	178.89	177.92	141.99
Dye 2	1.417	1.416	1.477	–	–	178.87	179.29	143.44
Dye 3	1.416	1.413	1.482	–	–	156.01	167.91	160.50
Dye 4	1.420	1.400	1.463	–	–	177.96	178.29	158.59
Dye 5	1.423	1.418	1.478	–	–	179.87	179.58	147.24
Dye 6	1.424	1.422	1.483	–	–	178.35	93.81	135.08
Dye 7	1.419	1.408	1.468	–	–	152.68	136.41	179.01
Dye 8	1.421	1.415	1.482	–	–	172.62	174.80	120.60
Dye 9	1.418	1.397	1.461	–	–	173.81	176.40	163.78

Table 2 The FMO energies of E_{HOMO-1}, E_{HOMO}, E_{LUMO}, E_{LUMO+1}, Δ_{H-L} (in eV), and μ_g (in Debye) at the CAM-B3LYP/6-31G(d,p) (LANL2DZ for Zn atom) level of the isolated dyes in THF with the CPCM

Dye	E_{HOMO-1}	E_{HOMO}	E_{LUMO}	E_{LUMO+1}	Δ_{H-L}	μ_g (D)
IDB-ZnP1	−6.205	−6.033	−1.503	−1.402	4.530	1.857
IDB-ZnP2	−6.187	−5.704	−1.478	−1.335	4.225	5.217
IDB-ZnP3	−6.258	−5.996	−1.789	−1.415	4.207	2.982
IDB-ZnP4	−6.250	−5.705	−1.737	−1.335	3.968	7.807
Dye 1	−6.244	−5.684	−1.722	−1.326	3.963	8.404
Dye 2	−6.285	−5.777	−2.056	−1.405	3.720	9.768
Dye 3	−6.303	−5.813	−2.219	−1.560	3.594	11.304
Dye 4	−6.232	−5.656	−1.749	−1.320	3.676	8.791
Dye 5	−6.218	−5.648	−1.716	−1.309	3.906	7.394
Dye 6	−6.298	−5.763	−1.886	−1.361	3.932	6.962
Dye 7	−6.264	−5.582	−2.245	−1.528	3.877	9.833
Dye 8	−6.246	−5.634	−2.070	−1.453	3.564	8.191
Dye 9	−6.257	−5.628	−1.952	−1.336	3.337	9.335

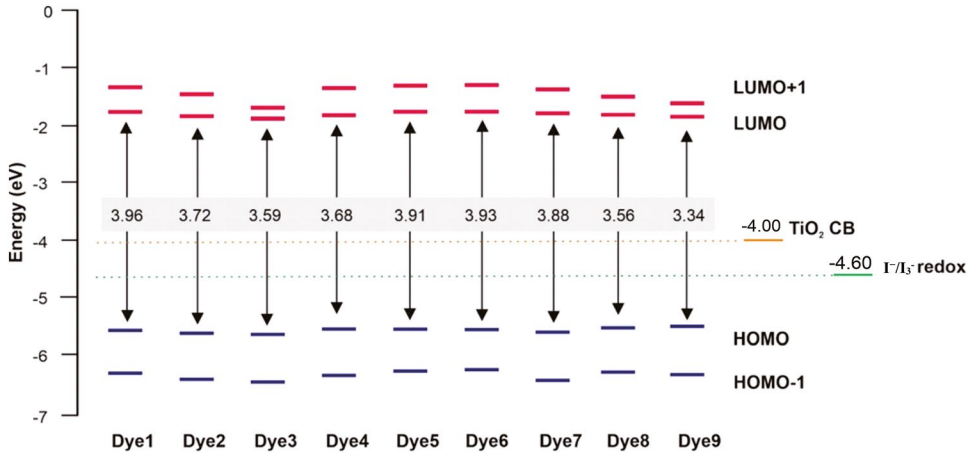

Fig. 3 Diagram of schematic energy for all dyes, TiO_2 CB, and I^-/I_3^- redox

The effective operation of DSSC sensitizers should meet the following criteria: a narrow bandgap with HOMO should be lower than the redox potential energy of the electrolyte I^-/I_3^- (−4.6 eV) to ensure that the dye can be efficiently regenerated by electron transfer from the redox mediator [60], whereas LUMO should be higher in the conduction band (CB) of TiO_2 (−4.0 eV) to ascertain that the dye can energetically allow an efficient interface charge injection from the excited state to the CB of the semiconductor [61]. Overall, as shown in Fig. 3, all dyes have a HOMO that lies below the redox potential of the electrolyte, whereas the LUMO of all dyes is above the CB of TiO_2. Therefore, it was observed that all dyes were energetically favorable for electron injection into the CB of TiO_2 and supported the effective regeneration by shuttle electrolytes [62].

Previous studies revealed that a decrease in LUMO and an increase in HOMO energy levels led to a lower energy gap, resulting in higher PCE observed experimentally [63]. In this case, the Δ_{H-L} energy values of the designed dye were studied and compared. The Δ_{H-L} energy values of the dyes studied increase in the order: Dye 1 > Dye 6 > Dye 5 > Dye 7 > Dye 2 > Dye 4 > Dye 3 > Dye 8 > Dye 9 (see Fig. 3 and Table 2). A smaller bandgap in the dye can lead to a higher short-circuit current density (J_{SC}) and thus a longer wavelength region [64]. The calculated results show that the elongation of the auxiliary acceptor in the dyes decreased the gap energy. In addition, Dye 9 has a lower gap value than other dyes, which is in line with previous studies reporting that the gap energy of the dye was reduced after inserting a suitable auxiliary acceptor [17]. Therefore, this reduction in Δ_{H-L} energy values confirms that the auxiliary acceptor of thieno[3,4-b]quinoxaline present in Dye 9 succeeds in reducing the energy values of Δ_{H-L}.

Figure 4 illustrates the distribution of frontier molecular orbitals (FMO) of the HOMO −1, HOMO, LUMO, and LUMO +1 levels of the studied dyes. The HOMO distribution of all dyes is very similar, which is delocalized over the entire Zn–porphyrin ring and extended to ethynyl units (for the D-π-A-A series) as a π bridge. Thus, Dye 1, Dye 3, Dye 4, and Dye 9, whose LUMO distribution is predominantly

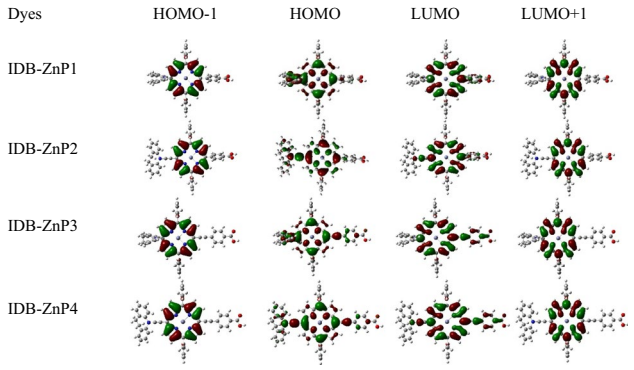

Fig. 4 The selected FMOs of the dyes between the ground state and the excited state, with an isodensity contour of 0.02

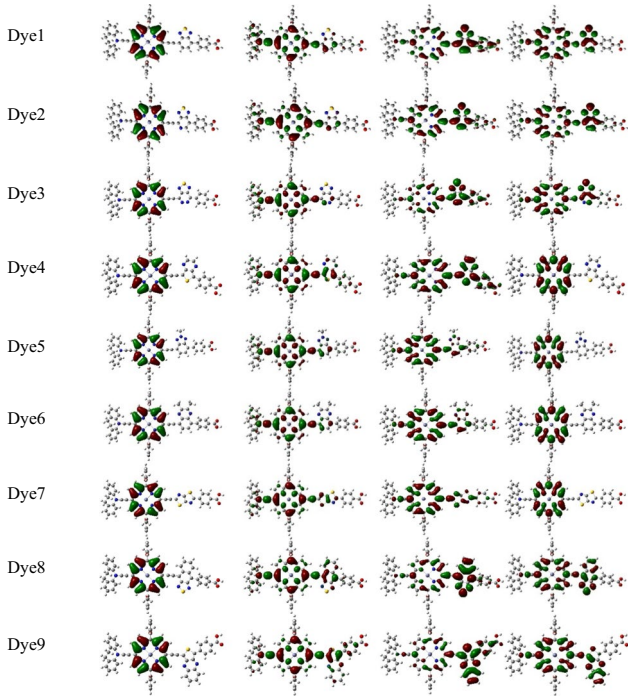

Fig. 4 (continued)

localized in the acceptor unit, contribute to the FMO distribution and the intramolecular charge transfer characters. Based on the above FMO illustrations, it can be inferred that the insertion of ethynyl and an auxiliary acceptor unit is a promising approach to obtain a bathochromic shift of the absorption band of the designed dyes, which is also consistent with the results of the electronic properties discussed above.

Considering the HOMO, LUMO, Δ_{H-L}, μg, and FMO, it can be concluded that Dye 9 and Dye 3 may have redshifted spectrums and better electron transition ability than other dyes, which should have the best photovoltaic performance.

3.3 Molecular orbital calculations

To determine the optical properties of the dyes, calculations in THF solvent were carried out using TD-DFT/CAM-B3LYP/6-31G(d,p) (LANL2DZ for Zn atoms) for the first 30 excited states. The calculated UV–Vis absorption wavelengths (λ), oscillator strength (f), excitation energies (ΔE), and the dominant transition configuration are provided in Table 3. The simulated UV–Vis spectra of the dyes are shown in Fig. 5.

The absorption spectrum of the dyes is characteristic of porphyrin, with high intensity (Soret band) in the range of λ 350–500 nm and negligible absorption (Q band) in the range of λ 550–700 nm [11–13]. Based on the observed data, our computational results indicate that the absorption band of porphyrin dye for the first expected excited state (Q-band, S_0-S_1) showed maximum oscillator power in the range of 600–800 nm, mainly from the HOMO → LUMO transition, so this typical intensity band is mainly analyzed. The second band (B-band) with lower intensity was found in the range of 400–600 nm. As expected, compared to IDB-ZnP1, IDB-ZnP4 dye using an ethynyl linker on the left and right sides of the meso-porphyrin showed a slight redshift. Compared to IDB-ZnP1, the absorption maxima of IDB-ZnP2, IDB-ZnP3, and IDB-ZnP4 were redshifted 27, 29, and 47 nm, respectively, while the corresponding f values also increased. This trend correlates with the conjugation length of π-linkers. It is worth mentioning that the ethynyl linker is useful for increasing the conjugation between donor and acceptor.

The oscillator strength (f) describes the strength of molecular interactions. The value of $f > 1$ represents a strong transition. In addition, greater oscillator strength (f) helps to improve light-harvesting efficiency (LHE) and leads to higher efficiency. As shown in Table 3, the f values of Dyes 1–9 were in the range of 0.7739 to 1.5463 a.u. compared to IDB-ZnP1 ($f = 0.0266$ a.u.). The results of f values for Dyes 1–9 show that all the designed dyes exhibit better performance, indicating that the introduction of the auxiliary acceptor is a promising strategy to increase efficiency due to higher LHE.

Moreover, the introduction of various auxiliary acceptor groups in Dyes1–9 significantly improved the LHE. The effect of the insertion of auxiliary acceptors on the absorption wavelengths can be seen from the simulated spectra (see Fig. 5). As listed in Table 4, it is noticed that Dye 9 obtaining thieno[3,4-b]quinoxaline as an auxiliary acceptor showed redshifted absorption and involved effective transition of HOMO → LUMO (82%). In addition, for Dyes 1–9, the maximum absorption wavelength of the Q band broad absorption led near the IR region relative to the IDB-ZnP4 (607.11 nm) with a simple dye with no inserted auxiliary acceptor and thus produced a redshifted absorption in the

Table 3 Electronic transitions, excitation energies ΔE (eV), maximum wavelength λ_{max} (nm), oscillator strength f (arb, units), and approximate transition assignment for the dyes

Dye	State	ΔE	λ_{max}	f	Approximate transition assignment
IDB-ZnP1	S_0-S_1	2.236	554.41	0.0266	H-1 → L + 1 (40%), H → L (57%)
	S_0-S_4	3.191	388.53	1.3071	H-1 → L (44%), H → L + 1 (52%)
	S_0-S_5	3.289	376.93	1.6433	H-2 → L (35%), H-1 → L + 2 (44%), H → L (20%)
IDB-ZnP2	S_0-S_1	2.133	581.26	0.2438	H-1 → L + 1 (27%), H → L (71%)
	S_0-S_3	3.066	404.37	2.0897	H-1 → L + 1 (67%), H → L (27%)
	S_0-S_4	3.136	395.40	1.4402	H-1 → L (61%), H → L + 1 (39%)
IDB-ZnP3	S_0-S_1	2.124	583.64	0.2681	H-1 → L + 1 (26%), H → L (71%)
	S_0-S_4	3.097	400.32	2.2461	H-2 → L (15%), H-1 → L + 1 (58%), H → L (19%)
	S_0-S_5	3.117	397.83	1.3881	H-1 → L (42%), H → L + 1 (56%)
IDB-ZnP4	S_0-S_1	2.042	607.11	0.6740	H-1 → L + 1 (17%), H → L (80%)
	S_0-S_3	3.018	410.88	2.2902	H → L + 1 (75%), H → L (17%)
	S_0-S_4	3.060	405.24	1.3793	H-1 → L (55%), H → L + 1 (45%)
Dye 1	S_0-S_1	1.928	643.08	0.8647	H-1 → L + 2 (13%), H → L (64%), H → L + 2 (19%)
	S_0-S_3	2.598	477.17	0.5814	H-1 → L + 2 (17%), H → L (24%), H → L + 1 (41%)
	S_0-S_4	2.960	418.88	1.1036	H-1 → L (52%), H → L + 2 (38%)
	S_0-S_5	3.045	407.21	1.4220	H-1 → L + 2 (62%), H → L + 1 (25%)
Dye 2	S_0-S_1	2.005	618.48	1.0873	H → L (67%), H → L + 1 (17%)
	S_0-S_3	2.573	481.78	0.6855	H-1 → L + 2(24%), H → L (17%), H → L + 1 (39%)
	S_0-S_4	2.942	421.48	0.8457	H-1 → L (50%), H → L + 2 (48%)
	S_0-S_5	3.032	408.98	1.0864	H-2 → L (14%), H-1 → L + 2 (49%), H → L + 1 (25%)
	S_0-S_6	3.274	378.70	0.5460	H-1 → L + 1 (62%)
Dye 3	S_0-S_1	1.901	652.35	1.5463	H → L (73%), H → L + 1 (16%)
	S_0-S_4	2.849	435.24	1.2498	H-1 → L + 1(41%), H → L + 2 (54%)
	S_0-S_5	2.947	420.68	1.3076	H-2 → L (12%), H-1 → L + 2(59%), H → L + 1 (22%)
Dye 4	S_0-S_1	1.853	669.16	1.3133	H → L (81%)
	S_0-S_4	2.968	417.68	1.1291	H-1 → L (53%), H → L (26%) H → L + 2 (17%)
	S_0-S_5	3.055	405.91	1.2644	H-2 → L (22%), H-1 → L + 1 (45%), H-1 → L + 2 (11%)
Dye 5	S_0-S_1	1.932	641.71	0.7965	H-1 → L + 1 (15%), H → L (73%)
	S_0-S_3	2.717	456.41	1.3422	H-1 → L + 1 (32%), H → L (17%), H → L + 2 (33%)
	S_0-S_4	2.950	420.37	1.1840	H-1 → L (54%), H → L + 1 (41%)
	S_0-S_5	3.052	406.19	0.8205	H-2 → L (14%), H-1 → L + 1 (46%), H → L + 2 (32%)
Dye 6	S_0-S_1	2.019	614.07	0.7739	H-1 → L + 1 (16%), H → L (80%)
	S_0-S_3	2.972	417.15	2.4681	H → L (69%), H → L + 2 (16%)
	S_0-S_4	3.051	406.39	1.3353	H-1 → L (55%), H → L + 1 (44%)
Dye 7	S_0-S_1	2.018	614.28	1.0686	H-1 → L + 2 (13%), H → L (81%)
	S_0-S_3	2.923	424.11	2.6554	H-1 → L + 1 (63%), H → L (12%), H → L + 2 (11%)
	S_0-S_4	3.040	407.85	1.3061	H-1 → L (49%), H → L + 1 (50%)
Dye 8	S_0-S_1	1.869	663.30	1.2797	H → L (77%)
	S_0-S_4	2.961	418.68	0.9226	H-1 → L (53%), H → L + 2 (41%)
	S_0-S_6	3.089	401.43	1.5251	H-1 → L + 2 (52%), H → L + 1 (33%)
Dye 9	S_0-S_1	1.638	756.72	1.3428	H → L (82%)
	S_0-S_5	2.857	434.94	0.6584	H-1 → L (61%), H → L + 2 (34%)
	S_0-S_6	3.016	411.10	2.0574	H-1 → L + 2 (69%), H → L + 1(20%)

following order: Dye 9 (756.7 nm) > Dye 8 (663.3 nm) > Dye 4 (669.2 nm) > Dye 3 (652.4 nm) > Dye 1 (643.1 nm) > Dye 5 (641.7 nm) > Dye 2 (618.5 nm) > Dye 7 (614.3 nm) > Dye 6 (614.1 nm). This corresponds to the order of the energy gaps of the dyes. The difference in the energy gap values and the spectral range of the dyes can be caused by the difference in the electron withdrawal ability of the auxiliary acceptors.

Among Dyes 1–9, Dye 9 with thieno[3,4-*b*]quinoxaline as a closed auxiliary acceptor for the barrier segment performed best at maximum wavelengths and energy gaps, whereas Dye 6 with 2,3-dimethylquinoxaline as auxiliary acceptor showed

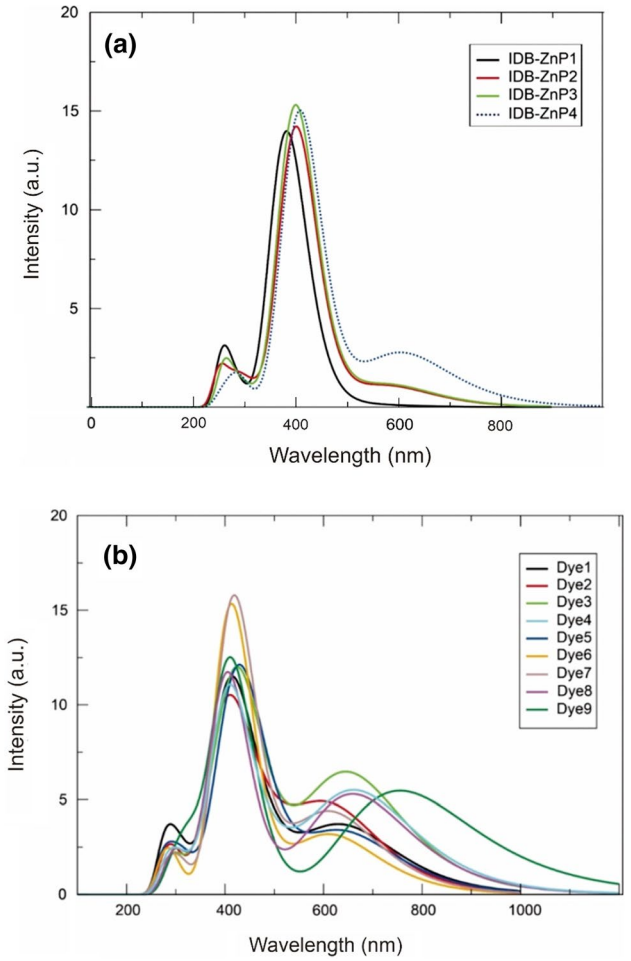

Fig. 5 The plot of the UV–Vis spectra of dyes **a** IDB-ZnP1 ~ 4 and **b** Dye1 ~ 9

gaps. It is recognized that a lower energy gap is expected to favor ICT. In general, this also confirms that the extension of the π-conjugated framework due to the presence of an additional co-acceptor moiety in the dyes is responsible for the reduction of the HOMO–LUMO gaps, which can also contribute to photon harvesting for the current conversion.

3.4 Electron injection and dye regeneration efficiency

It is necessary to discuss the suitability of the investigated dyes in the DSSCs. Of all the electrochemical parameters that can be optimized to achieve higher photoelectric conversion, the free energy of charge injection (ΔG_{inject}) from the dye in the excited state to the semiconductor CB and the free energy of dye are regenerated from reduced dye to I_3^- (ΔG_{reg}). The values of ΔG_{inject} and ΔG_{reg} can be expressed in the following equations:

$$\Delta G_{\text{inject}} = E^*_{\text{dye}} - E_{\text{CB}} \tag{1}$$

$$\Delta G_{\text{reg}} = E_{\text{dye}} - E_{I^-/I_3^-} \tag{2}$$

where $E_{\text{CB}} = -4.00$ eV is the conduction band of TiO_2 [65], and $E_{I^-/I_3^-} = -4.60$ eV is the potential of redox mediator of I^-/I_3^-. E_{dye} is defined as the ground-state oxidation potential of the dye which is considered to be equivalent to the HOMO energy, $E_{\lambda_{\max}}$ is the first transition energy corresponding to $\lambda_{\max}$, and E^*_{dye} is the excited-state oxidation potential calculated as [66]

$$E^*_{\text{dye}} = E_{\text{dye}} - \Delta E. \tag{3}$$

Table 4 Calculated E_{dye}, ΔE, E^*_{dye}, ΔG_{inject}, ΔG_{reg}, and LHE of the dyes

Dye	E_{dye}(eV)	ΔE(eV)	E^*_{dye}(eV)	ΔG_{inject}(eV)	ΔG_{reg}(eV)	LHE
IDB-ZnP1	6.033	2.236	3.797	−0.203	−1.433	0.059
IDB-ZnP2	5.704	2.133	3.571	−0.429	−1.104	0.430
IDB-ZnP3	5.996	2.124	3.871	−0.129	−1.396	0.461
IDB-ZnP4	5.705	2.042	3.662	−0.338	−1.105	0.788
Dye 1	5.684	1.928	3.756	−0.244	−1.084	0.863
Dye 2	5.777	2.005	3.772	−0.228	−1.177	0.918
Dye 3	5.813	1.901	3.912	−0.088	−1.213	0.972
Dye 4	5.628	1.853	3.776	−0.225	−1.028	0.951
Dye 5	5.656	1.932	3.724	−0.276	−1.056	0.840
Dye 6	5.648	2.019	3.629	−0.371	−1.048	0.832
Dye 7	5.763	2.018	3.744	−0.256	−1.163	0.915
Dye 8	5.634	1.869	3.765	−0.235	−1.034	0.947
Dye 9	5.582	1.638	3.943	−0.057	−0.982	0.955

the worst spectral properties. These observed absorption bands in the near-IR region correlate with small excitation energies (ΔE), which is associated with the HOMO–LUMO

The calculations for ΔE, ΔG_{inject}, and ΔG_{reg} are presented in Table 4; the findings showed that ΔG_{inject} values of the

designed dyes were negative, ranging from −0.05 to 0.50 eV. This can ensure the electron injection from the excited dye to the TiO_2 conduction band works smoothly. The ΔG_{reg} values of the designed dye were negative, which promoted the dye regeneration process and implied a low dye recombination [62]. In addition, all dyes showing heterocyclic barrier groups in the sensitizer indicate a reduction in excitation energies (ΔE) and hence a longer wavelength λ_{max}.

3.5 Overall efficiency

In this subsection, the energy conversion efficiency (η) of DSSC devices fabricated using the designed dyes is estimated primarily by their short-circuit current (J_{SC}), open-circuit photovoltage (V_{OC}), and fill factor (FF) values, as well as the intensity of the incident light (P_{inc}), can be calculated using the following Eq. (4)[67]:

$$\eta = \mathrm{FF}\frac{V_{OC}\,J_{SC}}{P_{inc}}. \tag{4}$$

Regarding this equation, where FF is defined as the ratio of the solar cell's maximum power and the product of J_{SC}, V_{OC}, and P_{inc}, the incidence of solar power in the cell. It is obvious that to increase efficiency, the modification of molecular structure effect on J_{SC} and V_{OC} products must be optimized.

$$V_{OC} = \frac{E_{CB}}{q} + \frac{k_B T}{q} ln\left[\frac{n_C}{N_{CB}}\right] - \frac{E_{redox}}{q}, \tag{5}$$

where $k_B\,T$ is the thermal energy, q is the electron charge, n_C is the number of electrons in the CB, N_{CB} is the accessible density from the CB state, and E_{redox} is the oxidation potential of the electrolyte [68].

V_{OC} is calculated by the energy difference between the CBE and the redox potential of the electrolyte. Typically, I^-/I_3^- is used as the redox electrolyte, so it is assumed to be constant. The primary factor influencing V_{OC} is ΔCBE, which can be expressed as Eq. (6):

$$\Delta\mathrm{CBE} = -\frac{q.\mu_g.\gamma}{\varepsilon_0.\varepsilon}, \tag{6}$$

where γ is the dyes surface concentration, and μ_g measures the component of the dipole moment of the individual molecule perpendicular to the semiconductor surface, and ε_0 and ε are the dielectric constants [69].

The Δ_{H-L} values of the designed dyes correlated with the μ_g values reported in Table 2. The calculated results show that the μ_g and Δ_{H-L} values followed the opposite trend. As the HOMO–LUMO gap value decreased, the μ_g value increased, which reflects better charge transport properties of the dyes. Indeed, Dye 9 and Dye 3 showed dipole moments of 9.335 Debye and 11.304 Debye, respectively, which were higher than those of other dyes. This high dipole moment indicates the polar nature of the dye molecule. Dyes with a larger dipole moment show better charge separation between the donor and acceptor units. As a result, the V_{OC} may increase with an increase in the concentration of acceptor species on the semiconductor surface [70]. Therefore, Dye 9 and Dye 3 may be the best candidates for achieving high conversion efficiency.

Equation (7) can be used to calculate the J_{SC} value of DSSCs:

$$J_{SC} = \int LHE(\lambda)\phi_{inject}\eta_{collect}d\lambda \tag{7}$$

where the LHE parameter indicates the ability of the dyes to efficiently harvest photons and evaluates the η of the DSSCs, ϕ_{inject} represents the electron injection efficiency, and $\eta_{collect}$ denotes the charge collection efficiency. The electrode is the same in all of the DSSCs under consideration, and only the dye as sensitizer differs. Therefore, we can assume that $\eta_{collect}$ is a constant [69].

Furthermore, it is well known that oscillator strength (f) reveals the LHE at a certain wavelength. The LHE value relates to the transition power for the excited states [71, 72], and can be calculated as Eq. (8):

$$\mathrm{LHE} = 1 - T = 1 - 10^{-A} = 1 - 10^{-f}. \tag{8}$$

As can be observed from Eq. (8), the significant f value is proportional to the maximum value of LHE obtained from the maximum photocurrent response. The LHE value has been found to be directly associated with the geometric structure of the studied dye, which should enhance the ICT (see Table 4). A higher degree of coplanarity tends to increase electronic conjugation between the electron donor and the electron acceptor, thereby increasing the f value [73]. It is clear that across the visible spectrum, dye molecules Dye 9 and Dye 3 showed a broader absorption spectrum than other dyes, with an estimated LHE value in the range of 0.96–0.97.

3.6 The ionization potential, electron affinity, and inner reorganization energy

To gain deeper insight into the effect of the additional π-linker and co-acceptor on the reactivity of the sensitizer, several parameters should be considered, including ionization potential (IP), electron affinity (EA), and reorganization energy (λ). The IP and EA are directly related to the energy barrier for hole and electron injection. It has been found that to achieve outstanding performance, a DSSC device should have good charge injection and transport properties, and equilibrium between the hole and electron transport.

Table 5 Calculated hole (λ_h) and electron (λ_e) reorganization energy, ionization potential (*IP*), and electron affinity (EA) of the dyes

Dyes	λ_h(eV)	λ_e(eV)	***IP***(eV)	***EA***(eV)
IDB-ZnP1	0.126	0.183	4.958	2.525
IDB-ZnP2	0.245	0.245	4.685	2.506
IDB-ZnP3	1.961	0.095	4.985	2.738
IDB-ZnP4	0.218	0.090	4.713	2.678
Dye 1	1.416	0.872	4.685	2.833
Dye 2	0.281	0.136	4.781	3.040
Dye 3	0.191	0.191	4.821	3.296
Dye 4	0.191	0.090	4.631	3.105
Dye 5	0.191	0.054	4.658	2.686
Dye 6	0.218	0.093	4.113	3.187
Dye 7	0.183	0.558	4.786	2.825
Dye 8	0.136	0.163	4.685	2.969
Dye 9	0.627	0.218	4.582	3.293

Table 6 The calculated intramolecular charge transfer (ICT) parameters of the dyes at the CAM-B3LYP/6-31G(d,p) (LANL2DZ for Zn atoms) level in THF with the CPCM

Dye	D_{CT}(Å)	$q_{CT}(e^-)$	H (Å)	t (Å)	$\Delta\mu_{CT}$(Debye)
IDB-ZnP1	1.028	0.184	4.525	−2.362	0.910
IDB-ZnP2	1.118	0.309	4.647	−2.501	1.657
IDB-ZnP3	0.568	0.319	4.650	−3.045	0.869
IDB-ZnP4	0.414	0.452	4.704	−3.395	0.897
Dye 1	2.061	0.495	5.513	−2.664	4.896
Dye 2	2.051	0.598	5.506	−2.706	5.896
Dye 3	2.932	0.654	5.762	−2.093	9.219
Dye 4	1.704	0.541	5.599	−3.118	4.481
Dye 5	0.418	0.466	4.899	−3.629	0.936
Dye 6	0.406	0.454	4.834	−3.551	0.886
Dye 7	0.648	0.519	5.018	−3.593	1.613
Dye 8	2.617	0.581	5.779	−2.387	7.302
Dye 9	3.681	0.630	5.913	−1.310	11.148

The adiabatic IP and EA values of the designed dyes can be expressed as follows [74]:

$$\mathrm{IP} = E^{+}(M_{+}) - E^{0}(M_{0}) \tag{9}$$

$$\mathrm{EA} = E^{0}(M_{0}) - E^{-}(M_{-}) \tag{10}$$

The IP, EA, λ_h, and λ_e are compared and listed in Table 5. Based on the computed adiabatic IP and EA values of Dyes 1–9 in the table, they show a range of 4.113–4.821 eV and 2.686–3.296 eV, respectively. The increase in EA implies that electron injection is more feasible between Dye 3 and Dye 9, demonstrating maximum EA values. This indicates that it has better electron transport properties. Moreover, Dye 6 and Dye 9 show lower IP values, which is beneficial for hole injection into semiconductors. The above discussions prove that the ethynyl linker with thieno[3,4-*b*]quinoxaline (Dye 9) is indeed more efficient, and results in lower ionization potential (IP) values and higher electron affinity (EA) values. These results also suggest that the smaller IP and higher EA values of Dye 9, among others, indicate that it is easy to inject holes and electrons into the HOMO and LUMO.

In addition to the *IP* and EA values, the charge transfer behavior can also be influenced by the intermolecular reorganization energy [34], which can be described in Eq. (11) and Eq. (12) by Marcus theory [75]:

$$\lambda_h = \left[E^{+}(M_{0}) - E^{+}(M_{+})\right] + \left[E^{0}(M_{+}) - E^{0}(M_{0})\right] \tag{11}$$

$$\lambda_e = \left[E^{-}(M_{0}) - E^{-}(M_{-})\right] + \left[E^{0}(M_{-}) - E^{0}(M_{0})\right] \tag{12}$$

Following these equations, $E^{+}(M_0)/E^{-}(M_0)$ is the energy of cation/anion in the optimized geometry of the neutral molecule, and $(E^{+}(M_{+})/E^{-}(M_0)/(E^{0}(M_0)$ is the energy of the cation/anion/neutral molecule in the corresponding optimized geometry, while $E^{0}(M_{+})/E^{0}(M_{-})$ is the energy of a neutral molecule in the optimized geometry of the cationic/anionic state. As displayed in Table 5, comparing the inner reorganization energies for electrons and holes, the values of λ_e are smaller than λ_h (except Dye 8). This indicates that the electron transferability in these dyes is better than their hole transferability [74, 75].

3.7 Charge transfer properties

To further ascertain whether the designed dye molecule can produce higher conversion efficiency, the excited-state charge transfer of the dye was also calculated, which results from the difference in the ground-state and excited-state charge density. The intramolecular charge transfer property is a key parameter to describe the photoelectric conversion property of the designed sensitizers. In general, electrons in the excited state at the donor need to be transferred to the acceptor. Suitable photo-induced intramolecular charge transfer can enhance effective charge separation [55, 57, 76, 77]. For this reason, the CT descriptors including the amount of charge transfer (q_{CT}), the effective charge transfer distance (D_{CT}), the corresponding alteration in the dipole moment ($\Delta\mu_{CT}$), and half of the sum of the centroid axis along the electron transfer (H) are described and summarized in Table 6. The electron density variation ($\Delta\rho$) from the excited state (ρ_{ES}) to the ground state (ρ_{GS}) can be calculated as follows [55]:

$$\Delta\rho(r) = \rho_{ES}(r) - \rho_{GS}(r) \tag{13}$$

where $\Delta\rho(r)$ can be divided into two parts: a positive ($\rho^+(r)$) and a negative ($\rho^-(r)$). The integrals of ρ^+ and ρ^- over all space should normally be equal. The positive (C^+) and negative (C^-) barycenter parts of these spatial regions can be computed as Eqs. (14–15):

$$C^+ = \frac{\int r\rho^+(r)dr}{q_{CT}} = \left(x^+, y^+, z^+\right), \tag{14}$$

$$C^- = \frac{\int r\rho^-(r)dr}{q_{CT}} = (x^-, y^-, z^-), \tag{15}$$

where q_{CT} is defined as the amount of charge transferred which can be obtained by integrating ρ^+ and ρ^- over all space. The value of q_{CT} is predicted to be in the range of 0–1 under one-electron excitation conditions. The D_{CT} parameter is defined as the distance the charge transfer traveled to determine the distance of the two-density depletion barycenters (positive and negative) of the density distribution in a molecule, and it can be calculated by Eq. (16):

$$D_{CT} = \left|C^+ - C^-\right| \tag{16}$$

In general, larger q_{CT} and D_{CT} resulting from the overlap between the holes and electrons are favorable for the ICT process. The amount of charge transferred (q_{CT}) can be obtained by integrating the increase or decrease in electron density in all spaces [78]. As shown in Table 6, the charge transfer effect of a dye is generated by introducing an auxiliary acceptor in the D-π-A-A porphyrin dye framework. Compared with IDB-ZnP1, Dye 2, Dye 9, and Dye 3 showed higher q_{CT} values of 0.598 e^- (Dye 2), 0.630 e^- (Dye 9), and 0.650 e^- (Dye 3). This indicates that the introduction of [1,2,5]thiadiazolo[3,4-*c*]pyridine, thieno[3,4-b]quinoxaline, and [1,2,5]thiadiazolo[3,4-*d*]pyridazine as auxiliary acceptors have a beneficial effect on the electron charge transfer in these dyes.

The value of *t* can be used to describe the spatial extent of a particular electronic transition. *t* with an axis value > 1.6 Å indicates that the applied function used in determining the CT model will not provide a precise description of the transition energy. A more detailed description of these descriptors can be found in previous works [55, 57, 76, 77]. The calculation results obtained a negative *t* value (*t* value < 1.6 Å) for all the studied dyes, and thus the applied function works well in describing the charge transfer model. These results are similar to observations reported in the literature [55, 79]. Their results suggest that there is an inevitable spatial proximity between areas of decreasing density and areas of increasing density. As the *t* value becomes larger, the overlap between the electron-donating and the electron-accepting regions decreases [79].

The dipole moment ($\Delta\mu_{CT}$) is another parameter to characterize how the dipole moment of the dye changes between the ground state (GS) and the excited state (ES) due to the electron transition [80]. Based on data in Table 6, Dye 8, Dye 3, and Dye 9 showed relatively higher $\Delta\mu_{CT}$ values of 7.302, 9.219, and 11.148 Debye, respectively. The value of $\Delta\mu_{CT}$ shows the variation in the molecular dipole moment between the ground state and the excited state due to electronic excitation. In general, during the ICT process, the density of positive and negative parts should be delocalized in the molecules of different groups. Thus, the reorganization of charge density increases the value of the dipole moment [80]. Moreover, *H* represents half of the totality of the barycenter axis along the charge direction. An *H* value greater than D_{CT} confirms that the overlap between the centers of mass along the *x*-axis of charge transfer is predictable [55].

3.8 Nonlinear optical (NLO) properties

One of the important keys in analyzing the charge transfer of molecules is assessing the efficiency of electronic communication between the acceptor and donor groups. In this case, by inducing the polarization of the applied external electric field, the response of the D-π-A system to the delocalization of the intramolecular charges on the donor and electron acceptor groups can be observed with the NLO properties [81]. Dyes with higher NLO properties possess better efficiency of intramolecular charge transfer. Thus, they will exhibit higher efficiency of DSSC photovoltaic performance [82].

The analysis of electric dipole moment (μ_{tot}) and components of NLO properties, including isotropic polarizability (α_0) and total first hyperpolarizability (β_{tot}), was carried out to comprehend the relationship between the structure and NLO characteristics. The calculated values of the resulting dipole moment, polarizability, and first hyperpolarizability using *x*,*y*,*z* (Cartesian) coordinates by CAM-B3LYP with LanL2DZ/6-31G(*d*,*p*) basis sets are tabulated in Table 7 and expressed as follows [50, 83]:

$$\mu_{tot} = \left(\mu_x^2 + \mu_y^2 + \mu_z^2\right)^{1/2} \tag{17}$$

$$\alpha_0 = \frac{1}{3}(\alpha_{xx} + \alpha_{yy} + \alpha_{zz}) \tag{18}$$

$$\beta_{tot} = \sqrt{\left(\beta_{xxx} + \beta_{xyy} + \beta_{xzz}\right)^2 + \left(\beta_{yyy} + \beta_{xxy} + \beta_{yzz}\right)^2 + \left(\beta_{zzz} + \beta_{xxz} + \beta_{yyz}\right)^2} \tag{19}$$

Table 7 The calculated electric dipole moment (μ_{tot}), the average polarizability (α_0) (10^{-24} esu), and the first hyperpolarizability β_{tot} (10^{-30} esu) of studied dyes

Dye	Dipole moment μ_{tot} (Debye)	Polarizability α_0 (10^{-24} esu)	First hyperpolarizability β_{tot} (10^{-30} esu)
IDB-ZnP1	1.492	119.226	63.398
IDB-ZnP2	4.460	129.069	327.866
IDB-ZnP3	2.426	131.962	295.762
IDB-ZnP4	6.544	143.758	741.079
Dye 1	7.197	167.366	1518.123
Dye 2	8.248	169.690	1979.103
Dye 3	9.476	170.173	2409.504
Dye 4	7.724	175.747	1773.069
Dye 5	6.493	166.578	1399.731
Dye 6	5.855	168.306	942.174
Dye 7	8.560	171.301	1453.136
Dye 8	7.139	180.335	1920.277
Dye 9	8.266	192.965	2627.878

As displayed in Table 7, Dye9 (8.266 Debye) and Dye 3 (9.476 Debye) are more polarized; thus, the μ_{tot} is also high. It is observed that Dye 9 and Dye 3 exhibit maximum linear to strong CT behavior caused by the introduction of auxiliary acceptors. As the auxiliary acceptor strength increases, the NLO performance decreases because of the strengthening of CT ability. A low molecular energy gap should facilitate greater interactions and therefore improve the polarization of the molecule. Furthermore, the molecular electric dipole moment can increase the microscopic polarization and hyperpolarization properties in relation to the applied field strength [84].

Introduction of different auxiliary acceptor units influenced the isotropic polarizability (α_{tot}) in Dye1 to Dye9. The highest value of isotropic polarizability was noted as 192.965×10^{-24} esu in Dye 9, followed by Dye 8 and Dye 4. This means that Dye 9 showed the best photoelectric properties, followed by Dye 8 and Dye 4. The isotropic polarizability values of the studied dyes are found to be in the following descending order: Dye 9 > Dye 8 > Dye 4 > Dye 3 > Dye 2 > Dye 7 > Dye 5 > Dye 1 > Dye 6 > IDB-ZnP4 > IDB-ZnP3 > IDB-ZnP2 > IDB-ZnP1.

In addition, the first hyperpolarizability values of the studied dyes are found to be in the following descending order: Dye 9 > Dye 3 > Dye 2 > Dye 8 > Dye 4 > Dye 1 > Dye 7 > Dye 5 > Dye 6 > IDB-ZnP4 > IDB-ZnP2 > IDB-ZnP3 > IDB-ZnP1. It is reflected that Dye 9 exhibits superior β_{tot} values compared to other derivatives, due to the low HOMO–LUMO bandgap, which promotes superior ICT properties. It is noteworthy that the NLO response of Dye 8 and Dye 9 containing naphtho[2,3-*c*][1,2,5]thiadiazole and thieno[3,4-*b*] quinoxaline as auxiliary acceptor was found to be higher than that of other dyes. For further evaluation, the highest NLO response was measured in Dye 9 with a β_{tot} value of 2627.878×10^{-30} esu. Compared to a standard NLO urea molecule [85, 86], the calculated value of the first hyperpolarizability of Dye 9 was 1747 times greater at the same theoretical level. Therefore, it can be concluded that the dye represents a potential NLO candidate for the fabrication of optoelectronic devices.

4 Conclusions

The optoelectronic and charge transfer properties of the D-π-A-A series for applications as a sensitizer in DSSCs were investigated in detail using DFT and TD-DFT calculations. The introduction of an auxiliary acceptor between the Zn–porphyrin ring and the anchoring group was found to have a significant positive effect in optimizing the distribution of electrons in molecular orbitals, reducing the HOMO–LUMO energy gap, and thereby broadening the absorption spectrum and increasing LHE values. Furthermore, a good balance between better-calculated energy levels, electron injection propulsion, dye regeneration energy, total reorganization energy, charge-transporting ability, and ICT parameters was obtained.

The computational results showed that the extended π-conjugation and high delocalization of the introduction of ethynyl linker and the auxiliary acceptors in Dye 9 improve performance mainly due to the favorable energy alignment between the HOMO dye and the redox potential of the electrolyte, leading to an efficient dye regeneration process. In addition, the designed molecule of Dye 9 exhibited smaller energy gaps, better ICT between electron donors and acceptors, and an enlarged absorption range in the NIR region. Dye 9 exhibited an appealingly large enhancement in NLO response through the ICT process, with a β_{tot} value that was many-fold higher than that of urea computed at the same theoretical level. It indicates that the studied dye molecules represent potential candidates for optoelectronic applications. Furthermore, we found that Dye 9 was the best among the studied dyes for the design of new sensitizers in DSSC applications.

Supplementary Information The online version contains supplementary material available at https://doi.org/10.1007/s10825-022-01851-7.

Acknowledgements One of the authors, L.A. Marlina, gratefully acknowledges the generous financial support provided by the Ministry of Research, Technology and Higher Education of the Republic of Indonesia through the *Program Pendidikan Magister Menuju Doktor untuk Sarjana Unggul* (PMDSU) Batch IV (6320/UN1/DITLIT/DIT-LIT/LT/2019). The authors also acknowledge the Research Directorate of Universitas Gadjah Mada for research funding under the *Rekognisi Tugas Akhir* (RTA) 2020 scheme.

Declarations

Conflict of interest The authors declare that they have no conflict of interest.

References

1. Zeng, J., Zhang, T., Zang, X., Kuang, D., Meier, H., Cao, D.: D-A-π-A organic sensitizers containing a benzothiazole moiety as an additional acceptor for use in solar cells. Sci. China Chem. **56**, 505–513 (2013). https://doi.org/10.1007/s11426-012-4758-8
2. O'Regan, B., Grätzel, M.: A low-cost, high-efficiency solar cell based on dye-sensitized colloidal TiO2 films. Nature **354**, 56–58 (1991)
3. Birel, Ö., Nadeem, S., Duman, H.: Porphyrin-based dye-sensitized solar cells (DSSCs): a review. J. Fluoresc. **27**, 1075–1085 (2017). https://doi.org/10.1007/s10895-017-2041-2
4. Jungsuttiwong, S., Tarsang, R., Sudyoadsuk, T., Promarak, V., Khongpracha, P., Namuangruk, S.: Theoretical study on novel double donor-based dyes used in high efficient dye-sensitized solar cells: The application of TDDFT study to the electron injection process. Org. Electron. **14**, 711–722 (2013). https://doi.org/10.1016/j.orgel.2012.12.018
5. Ahmad, S., Guillén, E., Kavan, L., Grätzel, M., Nazeeruddin, M.K.: Metal free sensitizer and catalyst for dye sensitized solar cells. Energy Environ. Sci. **6**, 3439–3466 (2013). https://doi.org/10.1039/c3ee41888j
6. AL-Temimei, F.A., OmranAlkhayatt, A.H.: A DFT/TD-DFT investigation on the efficiency of new dyes based on ethyl red dye as a dye-sensitized solar cell light-absorbing material. Optik (Stuttg). **208**, 163920 (2020). https://doi.org/10.1016/j.ijleo.2019.163920
7. Mathew, S., Yella, A., Gao, P., Humphry-Baker, R., Curchod, B.F.E., Ashari-Astani, N., Tavernelli, I., Rothlisberger, U., Nazeeruddin, M.K., Grätzel, M.: Dye-sensitized solar cells with 13% efficiency achieved through the molecular engineering of porphyrin sensitizers. Nat. Chem. **6**, 242–247 (2014). https://doi.org/10.1038/nchem.1861
8. Zhang, N., Zhang, B., Yan, J., Xue, X., Peng, X., Li, Y., Yang, Y., Ju, C., Fan, C., Feng, Y.: Synthesis of π-A-porphyrins and their photoelectric performance for dye-sensitized solar cells. Renew. Energy. **77**, 579–585 (2015). https://doi.org/10.1016/j.renene.2014.12.066
9. Ye, M., Wen, X., Wang, M., Iocozzia, J., Zhang, N., Lin, C., Lin, Z.: Recent advances in dye-sensitized solar cells: from photoanodes, sensitizers and electrolytes to counter electrodes. Mater. Today. **18**, 155–162 (2015). https://doi.org/10.1016/j.mattod.2014.09.001
10. Sheng, Y., Li, M., Flores-Leonar, M.M., Lu, W., Yang, J., Hu, Y.: Rational design of SM315-based porphyrin sensitizers for highly efficient dye-sensitized solar cells: a theoretical study. J. Mol. Struct. **1205**, 127567 (2020). https://doi.org/10.1016/j.molstruc.2019.127567
11. Guo, M., He, R., Dai, Y., Shen, W., Li, M., Zhu, C., Lin, S.H.: Electron-deficient pyrimidine adopted in porphyrin sensitizers: a theoretical interpretation of π-spacers leading to highly efficient photo-to-electric conversion performances in dye-sensitized solar cells. J. Phys. Chem. C. **116**, 9166–9179 (2012). https://doi.org/10.1021/jp2109829
12. Wang, Y., Chen, B., Wu, W., Li, X., Zhu, W., Tian, H., Xie, Y.: Efficient solar cells sensitized by porphyrins with an extended conjugation framework and a carbazole donor: from molecular design to cosensitization. Angew. Chemie - Int. Ed. **53**, 10779–10783 (2014). https://doi.org/10.1002/anie.201406190
13. Mahmood, A., Hu, J.Y., Xiao, B., Tang, A., Wang, X., Zhou, E.: Recent progress in porphyrin-based materials for organic solar cells. J. Mater. Chem. A. **6**, 16769–16797 (2018). https://doi.org/10.1039/c8ta06392c
14. Meti, P., Nagaraju, G., Yang, J.W., Jung, S.H., Gong, Y.D.: Synthesis of dipyrrolopyrazine-based sensitizers with a new π-bridge end-capped donor-acceptor framework for DSSCs: a combined experimental and theoretical investigation. New J. Chem. **43**, 3017–3025 (2019). https://doi.org/10.1039/c8nj06083e
15. Yao, Z., Zhang, M., Wu, H., Yang, L., Li, R., Wang, P.: Donor/acceptor indenoperylene dye for highly efficient organic dye-sensitized solar cells. J. Am. Chem. Soc. **137**, 3799–3802 (2015). https://doi.org/10.1021/jacs.5b01537
16. Song, X., Zhang, W., Li, X., Jiang, H., Shen, C., Zhu, W.H.: Influence of ethynyl position on benzothiadiazole based D-A-π-A dye-sensitized solar cells: spectral response and photovoltage performance. J. Mater. Chem. C. **4**, 9203–9211 (2016). https://doi.org/10.1039/c6tc03418g
17. Slimi, A., Fitri, A., Touimi Benjelloun, A., Elkhattabi, S., Benzakour, M., Mcharfi, M., Bouachrine, M.: Molecular design of D-π-A-A organic dyes based on triphenylamine derivatives with various auxiliary acceptors for high performance DSSCs. J. Electron. Mater. **48**, 4452–4462 (2019). https://doi.org/10.1007/s11664-019-07228-0
18. Zhao, D., Saputra, R.M., Song, P., Yang, Y., Ma, F., Li, Y.: Enhanced photoelectric and photocatalysis performances of quinacridone derivatives by forming D-π-A-A structure. Sol. Energy. **201**, 872–883 (2020). https://doi.org/10.1016/j.solener.2020.03.053
19. Cui, Y., Wu, Y., Lu, X., Zhang, X., Zhou, G., Miapeh, F.B., Zhu, W., Wang, Z.S.: Incorporating benzotriazole moiety to construct D-A-π-A organic sensitizers for solar cells: Significant enhancement of open-circuit photovoltage with long alkyl group. Chem. Mater. **23**, 4394–4401 (2011). https://doi.org/10.1021/cm202226j
20. Mao, J., Guo, F., Ying, W., Wu, W., Li, J., Hua, J.: Benzotriazole-bridged sensitizers containing a furan moiety for dye-sensitized solar cells with high open-circuit voltage performance. Chem. - An Asian J. **7**, 982–991 (2012). https://doi.org/10.1002/asia.201100967
21. Shi, J., Chai, Z., Su, J., Chen, J., Tang, R., Fan, K., Zhang, L., Han, H., Qin, J., Peng, T., Li, Q., Li, Z.: New sensitizers bearing quinoxaline moieties as an auxiliary acceptor for dye-sensitized solar cells. Dye. Pigment. **98**, 405–413 (2013). https://doi.org/10.1016/j.dyepig.2013.03.015
22. Pei, K., Wu, Y., Islam, A., Zhu, S., Han, L., Geng, Z., Zhu, W.: Dye-sensitized solar cells based on quinoxaline dyes: Effect of π-linker on absorption, energy levels, and photovoltaic performances. J. Phys. Chem. C. **118**, 16552–16561 (2014). https://doi.org/10.1021/jp412259t
23. Pei, K., Wu, Y., Li, H., Geng, Z., Tian, H., Zhu, W.H.: Cosensitization of D-A-π-A quinoxaline organic dye: Efficiently filling the absorption valley with high photovoltaic efficiency. ACS Appl. Mater. Interfaces. **7**, 5296–5304 (2015). https://doi.org/10.1021/am508623e
24. Chmovzh, T.N., Knyazeva, E.A., Tanaka, E., Popov, V.V., Mikhalchenko, L.V., Robertson, N., Rakitin, O.A.: [1,2,5] Thiadiazolo[3,4-d]Pyridazine as an internal acceptor in the D-A-_-A organic sensitizers for Dye-sensitized solar cells. Molecules **24**, 1588 (2019)
25. Wu, Y., Marszalek, M., Zakeeruddin, S.M., Zhang, Q., Tian, H., Grätzel, M., Zhu, W.: High-conversion-efficiency organic dye-sensitized solar cells: molecular engineering on D-A-π-A featured organic indoline dyes. Energy Environ. Sci. **5**, 8261–8272 (2012). https://doi.org/10.1039/c2ee22108j

26. Zhu, H., Li, W., Wu, Y., Liu, B., Zhu, S., Li, X., Ågren, H., Zhu, W.: Insight into benzothiadiazole acceptor in D-A-π-A configuration on photovoltaic performances of dye-sensitized solar cells. ACS Sustain. Chem. Eng. **2**, 1026–1034 (2014). https://doi.org/10.1021/sc500035j
27. Cheng, J.X., Huang, Z.S., Wang, L., Cao, D.: D-π-A-π-A featured dyes containing different electron-withdrawing auxiliary acceptors: The impact on photovoltaic performances. Dye. Pigment. **131**, 134–144 (2016). https://doi.org/10.1016/j.dyepig.2016.04.001
28. Chaurasia, S., Ni, J.S., Hung, W.I., Lin, J.T.: 2H-[1,2,3]Triazolo[4,5-c]pyridine cored organic dyes achieving a high efficiency: a systematic study of the effect of different donors and spacers. (2015)
29. Liyanage, N.P., Yella, A., Nazeeruddin, M., Grätzel, M., Delcamp, J.H.: Thieno[3,4-b]pyrazine as an electron deficient π-bridge in D-A-π-A DSCs. ACS Appl. Mater. Interfaces. **8**, 5376–5384 (2016). https://doi.org/10.1021/acsami.5b12503
30. Yen, Y.S., Ni, J.S., Hung, W.I., Hsu, C.Y., Chou, H.H., Lin, J.T.: Naphtho[2,3-c][1,2,5]thiadiazole and 2H-Naphtho[2,3-d][1,2,3]triazole-containing D-A-π-A conjugated organic Dyes for Dye-sensitized solar cells. ACS Appl. Mater. Interfaces. **8**, 6117–6126 (2016). https://doi.org/10.1021/acsami.6b00806
31. Zeng, W., Cao, Y., Bai, Y., Wang, Y., Shi, Y., Zhang, M., Wang, F., Pan, C., Wang, P.: Efficient dye-sensitized solar cells with an organic photosensitizer featuring orderly conjugated ethylenedioxythiophene and dithienosilole blocks. Chem. Mater. **22**, 1915–1925 (2010). https://doi.org/10.1021/cm9036988
32. Irfan, A., Aftab, H., Al-Sehemi, A.G.: Push-pull effect on the geometries, electronic and optical properties of thiophene based dye-sensitized solar cell materials. J. Saudi Chem. Soc. **18**, 914–919 (2014). https://doi.org/10.1016/j.jscs.2011.11.013
33. Yin, J.F., Velayudham, M., Bhattacharya, D., Lin, H.C., Lu, K.L.: Structure optimization of ruthenium photosensitizers for efficient dye-sensitized solar cells: a goal toward a " bright" future. Coord. Chem. Rev. **256**, 3008–3035 (2012). https://doi.org/10.1016/j.ccr.2012.06.022
34. Fahim, Z.M.E., Bouzzine, S.M., Youssef, A.A., Bouachrine, M., Hamidi, M.: Ground state geometries, UV/vis absorption spectra and charge transfer properties of triphenylamine-thiophenes based dyes for DSSCs: A TD-DFT benchmark study. Comput. Theor. Chem. **1125**, 39–48 (2018). https://doi.org/10.1016/j.comptc.2018.01.002
35. Aziz, H.A., Santoso, G.A., Mulya, F., Pranowo, H.D.: Molecular and electronic structure of some symmetrically meso-substituted Hg(II)-porphyrin complexes. Asian J. Chem. **29**, 2224–2226 (2017). https://doi.org/10.1200/JCO.2012.47.7141
36. Pranowo, H.D., Mulya, F., Aziz, H.A., Santoso, G.A.: Study of substituent effect on properties of platinum(II) porphyrin semiconductor using density functional theory. Indones. J. Chem. 18, 742–748 (2018). https://doi.org/10.22146/ijc.26121
37. Mulya, F., Santoso, G.A., Aziz, H.A., Pranowo, H.D.: Design a better metalloporphyrin semiconductor: a theoretical studies on the effect of substituents and central ions. AIP Conf. Proc. 1755, (2016). https://doi.org/10.1063/1.4958514
38. Fan, C., Zhang, B., Li, Y., Liang, Y., Xue, X., Feng, Y.: Application-oriented computational studies on a series of D-π-A structured porphyrin sensitizers with different electron-donor groups. Phys. Chem. Chem. Phys. **17**, 30624–30631 (2015). https://doi.org/10.1039/c5cp05625j
39. Hay, P.J., Wadt, W.R.: Ab initio effective core potentials for molecular calculations. Potentials for the transition metal atoms Sc to Hg. J. Chem. Phys. **82**, 270–283 (1985). https://doi.org/10.1063/1.448799
40. Luque, F.J., López, J.M., Orozco, M.: Perspective on "Electrostatic interactions of a solute with a continuum. A direct utilization of ab initio molecular potentials for the prevision of solvent effects." Theor. Chem. Acc. **103**, 343–345 (2000). https://doi.org/10.1007/s002149900013
41. Barone, V., Cossi, M.: Quantum calculation of molecular energies and energy gradients in solution by a conductor solvent model. J. Phys. Chem. A. **102**, 1995–2001 (1998). https://doi.org/10.1021/jp9716997
42. Cossi, M., Rega, N., Scalmani, G., Barone, V.: Energies, structures, and electronic properties of molecules in solution with the C-PCM solvation model. J. Comput. Chem. **24**, 669–681 (2003). https://doi.org/10.1002/jcc.10189
43. Lee, C., Yang, W., Parr, R.G.: Development of the Colle-Salvetti correlation-energy formula into a functional of the electron density. Phys. Rev. **37**, 785–789 (1988)
44. Yanai, T., Tew, D.P., Handy, N.C.: A new hybrid exchange-correlation functional using the Coulomb-attenuating method (CAM-B3LYP). Chem. Phys. Lett. **393**, 51–57 (2004). https://doi.org/10.1016/j.cplett.2004.06.011
45. Zhao, Y., Truhlar, D.G.: The M06 suite of density functionals for main group thermochemistry, thermochemical kinetics, noncovalent interactions, excited states, and transition elements: Two new functionals and systematic testing of four M06-class functionals and 12 other function. Theor. Chem. Acc. **120**, 215–241 (2008). https://doi.org/10.1007/s00214-007-0310-x
46. Salzner, U., Aydin, A.: Improved prediction of properties of π-conjugated oligomers with range-separated hybrid density functionals. J. Chem. Theory Comput. **7**, 2568–2583 (2011). https://doi.org/10.1021/ct2003447
47. Becke, A.D.: A new mixing of Hartree-Fock and local density-functional theories. J. Chem. Phys. **98**, 1372–1377 (1993). https://doi.org/10.1063/1.464304
48. Adamo, C., Barone, V.: Exchange functionals with improved long-range behavior and adiabatic connection methods without adjustable parameters: The mPW and mPW1PW models. J. Chem. Phys. **108**, 664–675 (1998). https://doi.org/10.1063/1.475428
49. Shkir, M.: Investigation on the key features of L-Histidinium 2-nitrobenzoate (LH2NB) for optoelectronic applications: a comparative study. J. King Saud Univ. - Sci. **29**, 70–83 (2017). https://doi.org/10.1016/j.jksus.2016.03.002
50. Hutama, A.S., Huang, H., Kurniawan, Y.S. Investigation of the chemical and optical properties of halogen-substituted N-methyl-4-piperidone curcumin analogs by density functional theory calculations. Spectrochim. Acta - Part A Mol. Biomol. Spectrosc. 221, 117152 (2019). https://doi.org/10.1016/j.saa.2019.117152
51. AlFaify, S., Shkir, M., Arora, M., Irfan, A., Algarni, H., Abbas, H., Al-Sehemi, A.G.: Quantum chemical investigation on molecular structure, vibrational, photophysical and nonlinear optical properties of l-threoninium picrate: an admirable contender for nonlinear applications. J. Comput. Electron. **17**, 1421–1433 (2018). https://doi.org/10.1007/s10825-018-1230-9
52. Shkir, M., AlFaify, S., Arora, M., Ganesh, V., Abbas, H., Yahia, I.S.: A first principles study of key electronic, optical, second and third order nonlinear optical properties of 3-(4-chlorophenyl)-1-(pyridin-3-yl) prop-2-en-1-one: a novel D- π -A type chalcone derivative. J. Comput. Electron. **17**, 9–20 (2018). https://doi.org/10.1007/s10825-017-1050-3
53. Shkir, M., Patil, P.S., Arora, M., AlFaify, S., Algarni, H.: An experimental and theoretical study on a novel donor-π-acceptor bridge type 2, 4, 5-trimethoxy-4′-chlorochalcone for optoelectronic applications: a dual approach. Spectrochim. Acta - Part A Mol. Biomol. Spectrosc. **173**, 445–456 (2017). https://doi.org/10.1016/j.saa.2016.09.022
54. Frisch, M.J., Trucks, G.W., Schlegel, H.B., Scuseria, G.E., Robb, M.A., Cheeseman, J.R., Scalmani, G., Barone, V., Mennucci, B., Petersson, G.A., Nakatsuji, H., Caricato, M., Li, X., Hratchian, H.P., Izmaylov, A.F., Bloino, J., Zheng, G.,

Sonnenberg, J.L., Hada, M., Ehara, M., Toyota, K., Fukuda, R., Hasegawa, J., Ishida, M., Nakajima, T., Honda, Y., Kitao, O., Nakai, H., Vreven, T., Montgomery Jr., J.A., Peralta, J.E., Ogliaro, F., Bearpark, M., Heyd, J.J., Brothers, E., Kudin, K.N., Staroverov, V.N., Kobayashi, R., Normand, J., Raghavachari, K., Rendell, A., Burant, J.C., Iyengar, S.S., Tomasi, J., Cossi, M., Rega, N., Millam, J.M., Klene, M., Knox, J.E., Cross, J.B., Bakken, V., Adamo, C., Jaramillo, J., Gomperts, R., Stratmann, R.E., Yazyev, O., Austin, A.J., Cammi, R., Pomelli, C., Ochterski, J.W., Martin, R.L., Morokuma, K., Zakrzewski, V.G., Voth, G.A., Salvador, P., Dannenberg, J.J., Dapprich, S., Daniels, A.D., Farkas, Ö., Foresman, J.B., Ortiz, J. V, Cioslowski, J., Fox, D.J.: Gaussian-09 Revision D.01. Gaussian, Inc., Wallingford, CT (2013)

55. Le Bahers, T., Adamo, C., Ciofini, I.: A qualitative index of spatial extent in charge-transfer excitations. J. Chem. Theory Comput. **7**, 2498–2506 (2011). https://doi.org/10.1021/ct200308m
56. Ciofini, I., Le Bahers, T., Adamo, C., Odobel, F., Jacquemin, D.: Through-space charge transfer in rod-like molecules: lessons from theory. J. Phys. Chem. C. **116**, 11946–11955 (2012). https://doi.org/10.1021/jp3030667
57. Lu, T., Chen, F.: Multiwfn: a multifunctional wavefunction analyzer. J. Comput. Chem. **33**, 580–592 (2012). https://doi.org/10.1002/jcc.22885
58. Mo, Y., Lin, Z., Wu, W., Zhang, Q.: Bond-distorted orbitals and effects of hybridization and resonance on C-C bond lengths. J. Phys. Chem. **100**, 11569–11572 (1996). https://doi.org/10.1021/jp953433a
59. Wazzan, N.A.: A DFT/TDDFT investigation on the efficiency of novel dyes with ortho-fluorophenyl units (A1) and incorporating benzotriazole/benzothiadiazole/phthalimide units (A2) as organic photosensitizers with D-A2–π–A1 configuration for solar cell applications. J. Comput. Electron. **18**, 375–395 (2019). https://doi.org/10.1007/s10825-019-01308-4
60. Zhang, G., Bai, Y., Li, R., Shi, D., Wenger, S., Zakeeruddin, S.M., Grätzel, M., Wang, P.: Employ a bisthienothiophene linker to construct an organic chromophore for efficient and stable dye-sensitized solar cells. Energy Environ. Sci. **2**, 92–95 (2009). https://doi.org/10.1039/b817990e
61. Mehmood, U., Hussein, I.A., Daud, M., Ahmed, S., Harrabi, K.: Theoretical study of benzene/thiophene based photosensitizers for dye sensitized solar cells (DSSCs). Dye. Pigment. **118**, 152–158 (2015). https://doi.org/10.1016/j.dyepig.2015.03.003
62. Zhang, C.R., Liu, L., Zhe, J.W., Jin, N.Z., Ma, Y., Yuan, L.H., Zhang, M.L., Wu, Y.Z., Liu, Z.J., Chen, H.S.: The role of the conjugate bridge in electronic structures and related properties of tetrahydroquinoline for dye sensitized solar cells. Int. J. Mol. Sci. **14**, 5461–5481 (2013). https://doi.org/10.3390/ijms14035461
63. Afolabi, S.O., Semire, B., Akiode, O.K., Afolabi, T.A., Adebayo, G.A., Idowu, M.A.: Design and theoretical study of phenothiazine-based low bandgap dye derivatives as sensitizers in molecular photovoltaics. Opt. Quantum Electron. (2020). https://doi.org/10.1007/s11082-020-02600-5
64. Xie, M., Bai, F.Q., Wang, J., Zheng, Y.Q., Lin, Z.: Theoretical investigations on the unsymmetrical effect of β-link Zn-porphyrin sensitizers on the performance for dye-sensitized solar cells. Phys. Chem. Chem. Phys. **20**, 3741–3751 (2018). https://doi.org/10.1039/c7cp07115a
65. Van Loon, E., Stroosnijder, L.: Evidences of hot excited state electron injection from sensitizer molecules to TiO2 nanocrystalline thin films. Res. Chem. Intermed. **27**, 393–406 (2001). https://doi.org/10.1163/156856701104202255
66. Sang-Aroon, W., Saekow, S., Amornkitbamrung, V.: Density functional theory study on the electronic structure of Monascus dyes as photosensitizer for dye-sensitized solar cells. J. Photochem. Photobiol. A Chem. **236**, 35–40 (2012). https://doi.org/10.1016/j.jphotochem.2012.03.014
67. Narayan, M.R.: Review: Dye sensitized solar cells based on natural photosensitizers. Renew. Sustain. Energy Rev. **16**, 208–215 (2012). https://doi.org/10.1016/j.rser.2011.07.148
68. Marinado, T., Nonomura, K., Nissfolk, J., Karlsson, M.K., Hagberg, D.P., Sun, L., Mori, S., Hagfeldt, A.: How the nature of triphenylamine-polyene dyes in dye-sensitized solar cells affects the open-circuit voltage and electron lifetimes. Langmuir **26**, 2592–2598 (2010). https://doi.org/10.1021/la902897z
69. Preat, J., Jacquemin, D., Perpète, E.A.: Towards new efficient dye-sensitised solar cells. Energy Environ. Sci. **3**, 891–904 (2010). https://doi.org/10.1039/c000474j
70. Hussain, R., Hassan, F., Khan, M.U., Mehboob, M.Y., Fatima, R., Khalid, M., Mahmood, K., Tariq, C.J., Akhtar, M.N.: Molecular engineering of A-D–C–D–A configured small molecular acceptors (SMAs) with promising photovoltaic properties for high-efficiency fullerene-free organic solar cells. Opt. Quantum Electron. **52**, 1–20 (2020). https://doi.org/10.1007/s11082-020-02482-7
71. Zhang, Z.L., Zou, L.Y., Ren, A.M., Liu, Y.F., Feng, J.K., Sun, C.C.: Theoretical studies on the electronic structures and optical properties of star-shaped triazatruxene/heterofluorene copolymers. Dye. Pigment. **96**, 349–363 (2013). https://doi.org/10.1016/j.dyepig.2012.08.020
72. Lu, X., Shao, Y., Wei, S., Zhao, Z., Li, K., Guo, C., Wang, W., Zhang, M., Guo, W.: Effect of the functionalized π-bridge on porphyrin sensitizers for dye-sensitized solar cells: an in-depth analysis of electronic structure, spectrum, excitation, and intramolecular electron transfer. J. Mater. Chem. C. **3**, 10129–10139 (2015). https://doi.org/10.1039/c5tc02286j
73. Chen, X., Jia, C., Wan, Z., Zhang, J., Yao, X.: Theoretical investigation of phenothiazine-triphenylamine-based organic dyes with different π spacers for dye-sensitized solar cells. Spectrochim. Acta - Part A Mol. Biomol. Spectrosc. **123**, 282–289 (2014). https://doi.org/10.1016/j.saa.2013.12.072
74. Zhan, C.G., Nichols, J.A., Dixon, D.A.: Ionization potential, electron affinity, electronegativity, hardness, and electron excitation energy: Molecular properties from density functional theory orbital energies. J. Phys. Chem. A. **107**, 4184–4195 (2003). https://doi.org/10.1021/jp0225774
75. Tavernier, H.L., Fayer, M.D.: Distance dependence of electron transfer in DNA: the role of the reorganization energy and free energy. J. Phys. Chem. B. **104**, 11541–11550 (2000). https://doi.org/10.1021/jp001362w
76. Ali, B.A., Allam, N.K.: Propping the optical and electronic properties of potential photo-sensitizers with different π-spacers: TD-DFT insights. Spectrochim. Acta - Part A Mol. Biomol. Spectrosc. **188**, 237–243 (2018). https://doi.org/10.1016/j.saa.2017.07.009
77. Andijani, N., Wazzan, N.A.: The effect of electron-donating substituents on tuning the nonlinear optical properties of pyrene-core arylamine derivatives: DFT calculations. Results Phys. **11**, 605–616 (2018). https://doi.org/10.1016/j.rinp.2018.10.002
78. Li, P., Cui, Y., Song, C., Zhang, H.: A systematic study of phenoxazine-based organic sensitizers for solar cells. Dye. Pigment. **137**, 12–23 (2017). https://doi.org/10.1016/j.dyepig.2016.09.060
79. Wu, H., Zhang, T., Wu, C., Guan, W., Yan, L., Su, Z.: A theoretical design and investigation on Zn-porphyrin-polyoxometalate hybrids with different π-linkers for searching high performance sensitizers of p-type dye-sensitized solar cells. Dye. Pigment. **130**, 168–175 (2016). https://doi.org/10.1016/j.dyepig.2016.03.025
80. Hosseinzadeh, E., Hadipour, N.L., Parsafar, G.: A computational investigation on the influence of different π spacer groups in the bithiazole-based organic dye sensitizers on the short-circuit photocurrent densities of dye-sensitized solar cells. J. Photochem. Photobiol. A Chem. **333**, 70–78 (2017). https://doi.org/10.1016/j.jphotochem.2016.10.010

81. Balanay, M.P., Kim, D.H.: Optical properties of porphyrin analogues for solar cells: An NLO approach. Curr. Appl. Phys. **11**, 109–116 (2011). https://doi.org/10.1016/j.cap.2010.06.028
82. Patil, D.S., Avhad, K.C., Sekar, N.: Linear correlation between DSSC efficiency, intramolecular charge transfer characteristics, and NLO properties – DFT approach. Comput. Theor. Chem. **1138**, 75–83 (2018). https://doi.org/10.1016/j.comptc.2018.06.006
83. Shkir, M., Alfaify, S., Abbas, H., Muhammad, S.: First principal studies of spectroscopic (IR and Raman, UV-visible), molecular structure, linear and nonlinear optical properties of l-arginine p-nitrobenzoate monohydrate (LANB): a new non-centrosymmetric material. Spectrochim. Acta—Part A Mol. Biomol. Spectrosc. 147, 84–92 . https://doi.org/10.1016/j.saa.2015.02.111
84. Patil, P.S., Shkir, M., Maidur, S.R., AlFaify, S., Arora, M., Rao, S.V., Abbas, H., Ganesh, V.: Key functions analysis of a novel nonlinear optical D-π-A bridge type (2E)-3-(4-Methylphenyl)-1-(3-nitrophenyl) prop-2-en-1-one chalcone: an experimental and theoretical approach. Opt. Mater. (Amst) **72**, 427–435 (2017). https://doi.org/10.1016/j.optmat.2017.06.038
85. Adant, C., Dupuis, M., Bredas, J.L.: Ab initio study of the nonlinear optical properties of urea: electron correlation and dispersion effects. Int. J. Quantum Chem. **56**, 497–507 (1995). https://doi.org/10.1002/qua.560560853
86. Shkir, M., Muhammad, S., AlFaify, S., Irfan, A., Patil, P.S., Arora, M., Algarni, H., Jingping, Z.: An investigation on the key features of a D-π-A type novel chalcone derivative for opto-electronic applications. RSC Adv. **5**, 87320–87332 (2015). https://doi.org/10.1039/c5ra13494c

Authors and Affiliations

Lala Adetia Marlina[1,2] · Winarto Haryadi[2] · Harno Dwi Pranowo[1,2]

✉ Harno Dwi Pranowo
harnodp@ugm.ac.id

[1] Austrian-Indonesian Centre for Computational Chemistry (AIC), Universitas Gadjah Mada, Sekip Utara, Yogyakarta 55281, Indonesia

[2] Department of Chemistry, Faculty of Mathematics and Natural Sciences, Universitas Gadjah Mada, Sekip Utara, Yogyakarta 55281, Indonesia